Synthesis of Equivalent Circuit of Wireless Power Transfer Device Using Homogenization-based FEM

Yoshitsugu Otomo[1], Yuki Sato[1], Shogo Fujita[1], and Hajime Igarashi[1], *Member, IEEE*

[1]Graduate School of Information Science and Technology, Hokkaido University, Sapporo, 060-0814, Japan

In this work, the multi-turn coil used in a wireless power transfer (WPT) device is modeled as a uniform material using the homogenization method to consider the proximity effect. By fitting the coil impedance to the numerical results, the Cauer equivalent circuit of the multi-turn coil is synthesized for design and optimization of the power circuits in the WPT device. It is shown that the results obtained from the equivalent circuit and measurement are in good agreement. Moreover, the impedance of a flat WPT coil composed of a Litz wire is shown to be accurately evaluated by the proposed method when contribution of capacitance is negligible.

***Index Terms*—Cauer circuit, Homogenization, Litz wire, Proximity effect, Wireless power transfer.**

I. Introduction

Wireless power transfer (WPT) has attracted great attentions for application in electric vehicles, biomedical devices, householder appliances and so on [1]-[4]. Increase in frequency is preferable to downsize the coil for the WPT system. This can result in, however, significant increase in the coil resistance due to the skin and proximity effects. To accurately evaluate the coil impedance considering these effects with the conventional finite element method (FEM), the coil must be subdivided into fine elements that are smaller than the skin depth. FE analysis of WPT devices, therefore, needs long computational time. To overcome this problem, the homogenization method for the FE analysis has been proposed [5]. In this method, a multi-turn coil is modeled as a uniform material with complex permeability in frequency domain.

When analyzing a WPT device including a multi-turn coil and power circuit with nonlinear circuit elements, time-domain analysis is required. The model order reduction techniques allow us to synthesize the equivalent circuit, which is effective for time-domain analysis, from the FE model of an electric machine which obeys the quasi-static Maxwell equations [7]-[9]. This method synthesizes the equivalent circuit from the rational polynomial of frequency derived from a system equation. However, when one models a machine with the complex permeability, which is a transcendental function of frequency, the system matrix becomes an implicit function of frequency. It is uneasy, thus, to derive the rational polynomial and also the equivalent circuit from the reduced order model.

In this work, for time-domain analysis of the WPT devices considering the skin and proximity effects, we synthesize its equivalent circuit using the homogenization-based FEM in three dimensions. The equivalent circuit is synthesized by curve fitting to the frequency responses computed by the FEM. A WPT device including a rectifier is analyzed by the proposed method, and the numerical results are compared with the measured data. Moreover, the proposed method is applied to the three-dimensional analysis of flat Litz-wire coils used in WPT. The novelties in this work are the following: (i) the homogenization-based FEM is extended to solve three-dimensional problems, (ii) it is shown that the properties of a WPT device can be accurately represented by a T circuit including three Cauer circuits to consider the eddy current effect, (iii) the Cauer circuit synthesized from the result of the homogenization-based FEM is shown to work well for time-domain analysis even when the external circuit includes nonlinearity, (iv) it is shown that the circuit parameters in the Cauer equivalent circuit of WPT can be determined so that its frequency response is as near to that of the homogenization-based FEM as possible.

Manuscript received June 27, 2017; Corresponding author: Y. Otomo (e-mail: otomo@em.ist.hokudai.ac.jp).

Digital Object Identifier (inserted by IEEE).

II. Formulation

A. Homogenization-based FEM

The proximity effect can effectively be treated by introducing the complex permeability $\dot{\mu}_\mathrm{r}$. When we consider a straight round wire immersed in time-harmonic uniform magnetic field, $\dot{\mu}_\mathrm{r}$ is given by [5]

$$\dot{\mu}_\mathrm{r} = \mu_\mathrm{r} \frac{J_1(z)}{zJ_0(z) - J_1(z)} \tag{1a}$$

$$z = a(1-\mathrm{j})/\delta \tag{1b}$$

where μ_r, J_0, J_1, a, j and δ denote the relative permeability of the round wire, zeroth and first order Bessel functions, radius of wire, imaginary unit and skin depth, respectively. Note that (1a) is valid when the wire curvature radius is sufficiently larger than a and wire cross section is nearly circular. The macroscopic complex permeability homogenized over the coil region can be obtained from the extended Ollendorff formula [5, 6]

$$\langle \dot{\mu} \rangle = \mu_0 \left\{ 1 + \frac{2\eta(\dot{\mu}_\mathrm{r} - 1)}{2 + (1-\eta)(\dot{\mu}_\mathrm{r} - 1)} \right\} \tag{2}$$

where μ_0, and η denote the permeability of vacuum and volume fraction, respectively.

We extend (2) for three-dimensional problems below. Let $\boldsymbol{\tau}_1$ be the unit vectors tangential to the wire and $\boldsymbol{\tau}_2$, $\boldsymbol{\tau}_3$ be the unit

vectors orthogonal to $\boldsymbol{\tau}_1$. The magnetic permeability of the coil is set to μ_0 in parallel to $\boldsymbol{\tau}_1$, while it is set to $\langle\dot{\mu}\rangle$ on the plane spanned by $\boldsymbol{\tau}_2$, $\boldsymbol{\tau}_3$. In this coordinates, the magnetic reluctance tensor is given by $\boldsymbol{\nu} = \mathrm{diag}[1/\mu_0, 1/\langle\dot{\mu}\rangle, 1/\langle\dot{\mu}\rangle]$. The magnetic induction is represented as $\boldsymbol{B} = \Sigma_j B_j' \boldsymbol{\tau}_j$. The components are represented in terms of the Cartesian components in the form $B_i' = \Sigma_j T_{ij} B_j$. Hence, the reluctance tensor obeys the transformation T^t**ν**T.

When there is no conductor except the coil, we solve the magnetostatic equation including **ν**,

$$\mathrm{rot}\boldsymbol{\nu}(\mathrm{rot}\boldsymbol{A}) - \boldsymbol{J} = 0 \tag{3}$$

where $\boldsymbol{A}$ and $\boldsymbol{J}$ denote the vector potential and current density, respectively. When there are other conductors, an eddy current term is included in (3). Moreover, the circuit equations of the power transmission and receiving coils

$$\frac{R_k z J_0(z)}{2 J_1(z)} I_k + \mathrm{j}\omega \Phi_k = V_k \tag{4}$$

are coupled with (3), where R_k, I_k, Φ_k, V_k (k = 1,2) and ω denote the DC resistance, circuit current, interlinkage flux, input voltage and angular frequency, respectively. The first term in (4) includes the impedance due to the skin effect. The FE discretization of (3) and (4) leads to

$$\sum_j A_j \int_\Omega (\mathrm{rot}\boldsymbol{N}_i)^t \mathrm{T}^t \boldsymbol{\nu} \mathrm{T} (\mathrm{rot}\boldsymbol{N}_j) d\Omega - \sum_k I_k \int_{\Omega_C} \boldsymbol{N}_i \cdot \boldsymbol{j}_k d\Omega = 0 \tag{5a}$$

$$\frac{R_k z J_0(z)}{2 J_1(z)} I_k + \mathrm{j}\omega \sum_j A_j \int_{\Omega_C} \boldsymbol{N}_j \cdot \boldsymbol{j}_k d\Omega = V_k \tag{5b}$$

where $\boldsymbol{N}_i$, N_j and $\boldsymbol{j}_k$ denote the vector and scalar interpolation functions, unit current density of k-th coil, $\boldsymbol{j}_k = \boldsymbol{J}_k / I_k$.

B. Synthesis of equivalent circuit

We consider here a simple WPT device shown in Fig. 1 including a pair of ring coils, which can be considered as a transformer. Because the major radius, $D_{in}/2$, is much larger than the strand radius a, (1) and (2) would hold in this WPT. Moreover, (3) reduced to the two-dimensional equation including the scalar permeability $\langle\dot{\mu}_r\rangle$. WPT can be modeled by the equivalent circuit shown in Fig. 2. Note that impedances, $\dot{Z}_1$, $\dot{Z}_2$ and $\dot{Z}_M$, include the effects coming from eddy currents. They can be determined by solving (5), that is, $\dot{Z}_1 = \dot{V}_1/\dot{I}_1$, $\dot{Z}_M = \dot{V}_2/\dot{I}_1$ for $\dot{I}_2 = 0$, and $\dot{Z}_2 = \dot{V}_2/\dot{I}_2$ for $\dot{I}_1 = 0$.

We represent the coil impedance by the Cauer circuit shown in Fig. 3 [7]-[9]. Note here that the circuit parameters in the Cauer circuit has the following physical meaning: at sufficiently low frequencies, almost no current goes through R_2 but L_1. This means that R_1 and L_1 correspond to the DC resistance and inductance of the coil without eddy currents. When increasing frequency, eddy current loss and its diamagnetic effect appear, and they are represented by R_2 and L_2. The effects at higher frequencies are represented by R_k and L_k, $k \geq 3$. There exists one-to-one correspondence between the Cauer circuit and continued fraction. The impedance function in the Cauer circuit shown in Fig. 2 is now represented by

$$Z_k(s) - Z_M(s) = R_k^{DC} + \cfrac{1}{\cfrac{1}{sL_k^S} + \cfrac{1}{R_{k1} + \cfrac{1}{sL_{k2}} + \cdots}} \tag{6a}$$

$$Z_M(s) = \cfrac{1}{\cfrac{1}{sM_3} + \cfrac{1}{R_{31} + \cfrac{1}{sL_{32}} + \cdots}} \tag{6b}$$

where R_k^{DC}, L_k^S and M_3 denote the DC coil resistance and inductance of kth-coil in the T circuit, and mutual inductance, respectively, which are determined from static FE analysis. The T circuit shown in Fig. 2 is represented by the three Cauer circuits as shown in Fig. 4. The circuit parameters $\boldsymbol{R}_q = [R_{qj}]^t$, $\boldsymbol{L}_q = [L_{qj}]^t$, j=1, 2,… are determined by solving the optimization problems defined by

$$f(\boldsymbol{R}_q, \boldsymbol{L}_q) = \sqrt{\sum_i^m \left| Z_q^{FEM}(\omega_i) - Z_q(\omega_i, \boldsymbol{R}_q, \boldsymbol{L}_q) \right|^2} \to \min., \tag{7}$$

$$q = 1,2,3, \ \text{sub. to } R_{qj}, L_{qj} \geq 0$$

where $Z_q^{FEM}(\omega_i)$ denotes $\dot{Z}_1 - \dot{Z}_M$, $\dot{Z}_2 - \dot{Z}_M$ and $\dot{Z}_M$ obtained by the homogenization-based FEM, $Z_q(\omega_i, \boldsymbol{R}_q, \boldsymbol{L}_q)$ is the corresponding impedances computed from the Cauer circuit, and m is the number of sampling points for fitting.

TABLE I
SPACIFICATIONS OF SIMPLE WPT MODEL

Strand radius a	0.15 mm
Gap h	10.0 mm
Inner diameter D_{in}	60.0 mm
Outer diameter D_{out}	64.8 mm

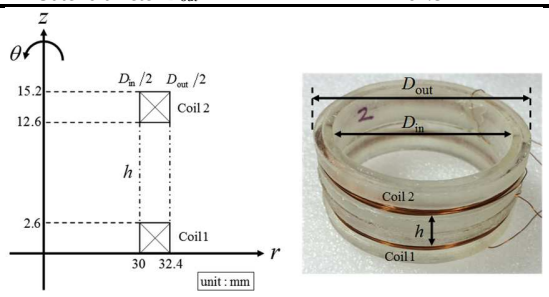

Fig. 1 Simple WPT model

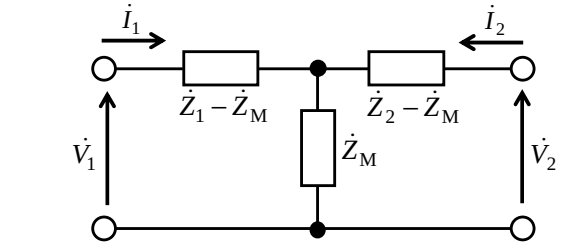

Fig. 2 T equivalent circuit

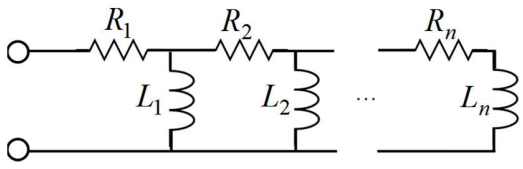

Fig. 3 Cauer circuit

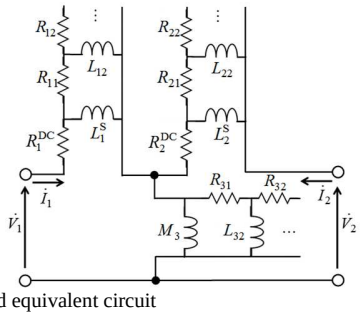

Fig. 4 Proposed equivalent circuit

III. Numerical Results

A. Frequency characteristics

TABLE II summarizes the fitting error between the synthesized equivalent circuit and the homogenization-based FEM. Because the error cannot be significantly reduced by increasing the stage number from 3 to 4, we employ the three-stage equivalent circuit in the following analysis. TABLE III summarizes the identified circuit parameters in Fig. 4. From the resultant frequency characteristics shown in Fig. 5, we find that the results obtained from the synthesized equivalent circuit and measurement are in good agreement. Because the skin depth is about 0.15 mm at the highest frequency, the proximity effect is more dominant than the skin effect. Thus, it is essentially important to introduce the complex permeability which represents the proximity effect.

TABLE II
NUMBER OF STAGE OF THE CIRCUIT AND FITTING ERROR

Stage	Error
2	3.8 %
3	0.3 %
4	0.2 %

TABLE III
OPTIMIZATION RESULTS OF EACH CIRCUIT ELEMENT

R_1^{DC}, R_2^{DC}	R_{11}, R_{21}	R_{12}, R_{22}	R_{31}	R_{32}
2.37 Ω	9.34×10^{3} Ω	5.16×10^{4} Ω	1.19×10^{5} Ω	2.34×10^{5} Ω
L_1^S, L_2^S	L_{12}, L_{22}	L_{13}, L_{23}	M_3	L_{32}
2.18×10^{-4} H	2.73×10^{-3} H	4.26×10^{-1} H	9.83×10^{-5} H	2.70×10^{-2} H
L_{33}				
3.02×10^{-4} H				

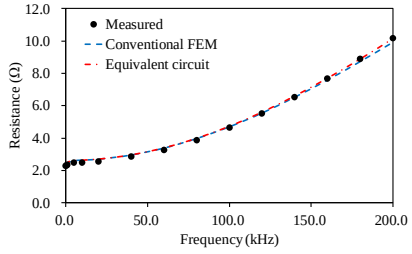

(a) Real part

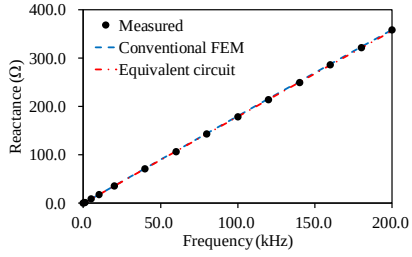

(b) Imaginary part

Fig. 5 Frequency dependence of coil impedance in WPT shown in Fig. 1

B. Quality factor

The quality factor of WPT is usually determined by $Q = \omega L/R_{DC}$ [10]-[12]. However, the actual Q value would be lower than this ideal Q which does not include eddy current losses. Using the present method, we evaluate Q, defined by the ratio $\mathrm{Im}(\dot{Z}_1)/\mathrm{Re}(\dot{Z}_1)$, to consider eddy currents. The computed values of Q are plotted in Fig. 6. From the results, we can see that Q reduces significantly due to the eddy currents especially when frequency is higher than 30 kHz.

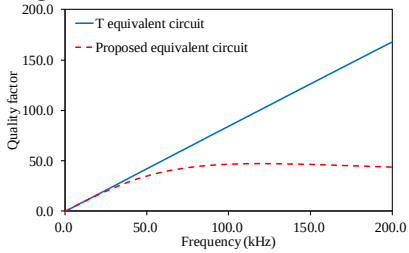

Fig. 6 Frequency dependence of quality factor

C. Time response

The primal and secondary WPT coils shown in Fig. 1 are connected to a voltage source and rectifying circuit, respectively. The proposed and conventional equivalent circuits are shown in Fig. 7. The parameters are set as follows: f=150 kHz, C_k=3.56 nF (k=1,2), C=1.0 mF, R_{LOAD}=300 Ω. In addition, SB340L is employed for the rectifier. The time response of this system is computed and also measured. The resultant diode and output voltages are plotted in Fig. 8. The errors in the output voltage from the measured value are summarized in TABLE IV. It is concluded from these results that the proposed method gives more accurate results in comparison with the conventional equivalent circuit.

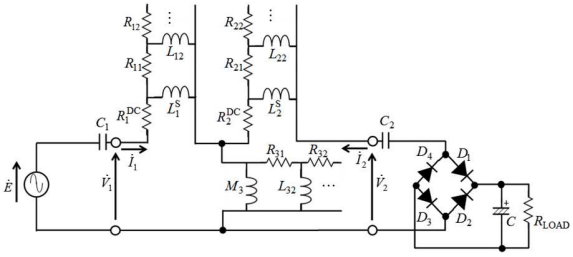

(a) Proposed

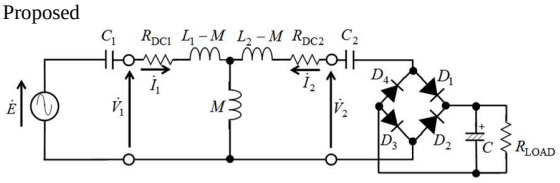

(b) Conventional (L_1, L_2=316.2 μH, M=98.3 μH)

Fig. 7 Equivalent circuits for WPT device

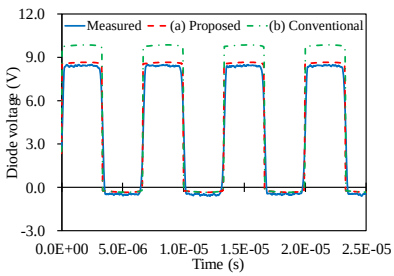

(a) Diode voltage

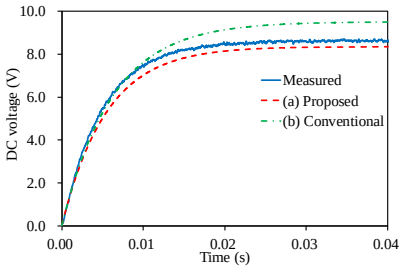

(b) Output DC voltage

Fig. 8 Time response of WPT shown in Fig. 1

TABLE IV
ERROR IN OUTPUT DC VOLTAGE

Proposed	–1.8 %
Conventional	11.8 %

IV. THREE-DIMENSIONAL ANALYSIS OF LITZ-WIRE COIL

We apply the proposed method to analysis of flat Litz-wire coil pairs, shown in Fig. 9, whose configuration is often used in real WPT systems. The coil parameters are summarized in TABLE V. Because of the assumed misalignment, three-dimensional FE analysis is required. There are 2,000 stranded wires in total. Conventional FEM would need quite a long computational time to compute the eddy currents in this system. In contrast, in the proposed method which solves (5), the coils are modeled by homogenous materials that can be analyzed with relatively coarse FE elements. The frequency dependences of the coil impedance for different misalignment computed by the proposed equivalent circuit are plotted in Fig. 10. We can see that the numerical results are in good agreement with measured values up to about 600 kHz. The discrepancy at frequencies higher than 600 KHz would come from the capacitance among the Litz wire. Consideration of this effect remains for future work. Moreover, the frequency dependences of the coil resistance for different tilt angles θ, expressed by the equivalent circuit shown in Fig.4, are plotted in Fig. 11. It can be seen that increase in θ reduces the resistance because of decrease in the interlinkage flux.

V. CONCLUSION

In this paper, we have proposed the equivalent circuit synthesized from the homogenization-based FEM to consider the eddy current losses for WPT devices. The proposed T equivalent circuit provides more accurate responses in comparison with the conventional T equivalent circuit. Moreover, using the proposed method, the effect of the misalignment of Litz-wire coils can effectively and accurately be evaluated.

TABLE V
SPECIFICATIONS OF LITZ-WIRE COILS

Strand radius	0.025 mm
Number of strands	50
Number of turns	40
Gap h	10 mm
Inner diameter D_{in}	30 mm
Outer diameter D_{out}	74 mm
Misalignment Δ	20, 30 mm
Tilt θ	10, 20 deg

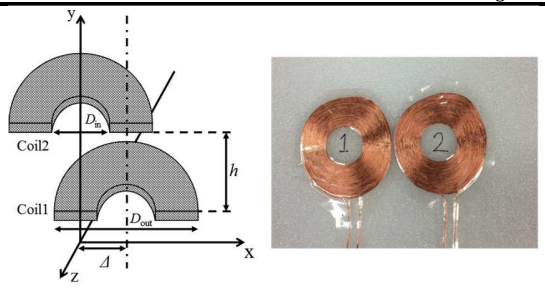

Fig. 9 Analysis of misalignment in WPT with Litz-wire coils

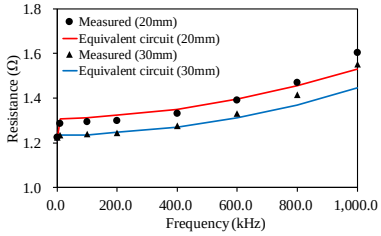

Fig. 10 Frequency dependence of WPT shown in Fig. 9

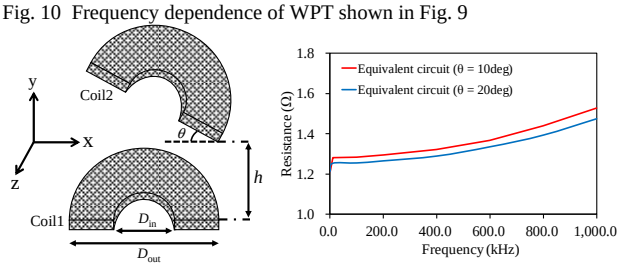

Fig. 11 Frequency dependence of WPT for different tilt angles

REFERENCES

[1] Y. Nagatsuka, N. Ehara, Y. Kaneko, S. Abe and T. Yasuda, "Compact Contactless Power Transfer System for Electric Vehicles," *2010 International Power Electronics Conference*, pp. 807-813, 2010.

[2] Z. Yang, W. Liu, and E. Basham, "Inductor Modeling in Wireless Links for Implantable Electronics," *IEEE Trans. Magn.*, vol. 43, no. 10, pp. 3851-3860, 2007.

[3] S. Hasanzadeh, S. Vaez-Zadeh and A. H. Isfahani, "Optimization of a Contactless Power Transfer System for Electric Vehicles," *IEEE Trans. Veh. Technol.*, vol. 61, no. 8, pp. 3566-3573, 2012.

[4] D. Kürschner, C. Rathge and U. Jumar, "Design Methodology for High Efficient Inductive Power Transfer Systems With High Coil Positioning Flexibility," *IEEE Trans. Ind. Electron.*, vol. 60, no. 1, pp. 372-381, 2013.

[5] H. Igarashi, "Semi-Analytical Approach for Finite Element Analysis of Multi-turn Coil Considering Skin and Proximity Effects," *IEEE Trans. Magn.*, vol. 53, no. 1, Art. 7400107, 2017.

[6] F. Ollendorff, "Magnetostatik der Massekerne," *Arch. f. Electrotechnik.*, 25, pp. 436-447, 1931.

[7] T. Shimotani, Y. Sato, and H. Igarashi, "Equivalent-Circuit Generation from Finite Element Solution Using Proper Orthogonal Decomposition," *IEEE Trans. Magn.*, vol. 52, no. 3, Art. 7206804, 2016.

[8] T. Shimotani, Y. Sato, and H. Igarashi, "Direct synthesis of equivalent circuits from reduced FE models using proper orthogonal decomposition," *COMPEL*, vol. 35, Iss. 6, pp. 2035-2044, 2016.

[9] Y. Sato, T. Shimotani, and H. Igarashi, "Synthesis of Cauer-Equivalent Circuit Based on Model Order Reduction Considering Nonlinear Magnetic Property," *IEEE Trans. Magn.*, vol.53, no. 6, Art. 1100204, 2017.

[10] Y. Ota, T. Takura, F. Sato, H. Matsuki, and T. Nonaka, "Impedance Matching Method About Multiple Contactless Power Feeding System for Portable Electronic Devices," *IEEE Trans. Magn.*, vol. 47, no. 10, pp. 4235-4237, 2011.

[11] S. Chopra, P. Bauer, "Analysis and Design Considerations for a Contactless Power Transfer System," *Telecommunications Energy Conference(INTELEC)*, DOI: 10.1109/INTLEC.2011.6099774, 2011.

[12] A. J. Moradewicz, M. P. Kazmierkowski, "Contactless Energy Transfer System With FPGA-Controlled Resonant Converter," *IEEE Trans. Ind. Electron.*, vol. 57, no. 9, pp. 3181-3190, 2010.